Electrical effects of metal nanoparticles embedded in ultra-thin colloidal quantum dot films

F. J. Beck, F. P. Garcia de Arquer, M. Bernechea, and G. Konstantatos

Citation: Appl. Phys. Lett. **101**, 041103 (2012); doi: 10.1063/1.4738993

View online: http://dx.doi.org/10.1063/1.4738993

View Table of Contents: http://apl.aip.org/resource/1/APPLAB/v101/i4

Published by the American Institute of Physics.

Electrical effects of metal nanoparticles embedded in ultra-thin colloidal quantum dot films

F. J. Beck, F. P. Garcia de Arquer, M. Bernechea, and G. Konstantatos
ICFO - The Institute of Photonic Sciences, Mediterranean Technology Park, 08860 Castelldefels, Barcelona, Spain

(Received 1 June 2012; accepted 9 July 2012; published online 23 July 2012)

Plasmonic light trapping can increase the absorption of light in thin semiconductor films. We investigate the effect of embedded metal nanoparticle (MNP) arrays on the electrical characteristics of ultra-thin PbS colloidal quantum dot (CQD) photoconductors. We demonstrate that direct contact with the metal nanoparticles can suppress or enhance the photocurrent depending on the work function of the metal, which dominates the optical effects of the particles for ultra-thin films. These results have implications for designing plasmonic CQD optoelectronic devices. © *2012 American Institute of Physics*. [http://dx.doi.org/10.1063/1.4738993]

Colloidal quantum dots (CQDs) are a promising material system for optoelectronics.[1,2] In particular, PbS CQDs have attracted significant attention as the exciton peak can be tuned from the visible to the near infra-red. These materials can be manufactured in the solution phase and spin-cast to form dense semiconductor films on a variety of substrates, reducing the cost of device fabrication. PbS CQD based devices have already demonstrated record performances for photoconductors,[3] and solar cells with efficiencies of up to 6%.[4] However, due to short carrier lifetimes and diffusion lengths, the thickness of the active region is restricted to a few hundred nanometers to maintain high carrier extraction efficiency, resulting in devices that are limited by non-complete absorption. This restriction can be lifted by employing light trapping techniques to increase the absorption in the active layer. Plasmonic light trapping is particularly interesting for CQD solar cells as these materials offer the potential to easily incorporate metallic nanostructures inside the active region. Recently, we have demonstrated photocurrent enhancements of up to a factor of 2.4 near the band edge in 450 nm thick PbS CQD photodetectors employing random Ag nanoparticle arrays.[5]

In the last decade, advances in plasmonics for light trapping[6] in solar cells and other optoelectronic devices have demonstrated significant photocurrent enhancement in a number of material systems.[7–12] In the majority of the studies published, the strong interaction between propagating light fields and metal nanostructures is exploited to scatter incident light and couple it efficiently into absorber layers. For example, Ferry and co-workers have demonstrated short circuit current enhancements exceeding those of standard Lambertian type texturing, by employing scattering nano-patterned back contacts in ultra-thin a:Si solar cells.[8] Studies have also demonstrated absorption enhancement in thin active layers by taking advantage of the enhanced electric fields in the vicinity of optically excited localised surface plasmons on metal nanoparticles (MNP); the so called near-field effect.[13–15] As suggested recently by Pala and colleagues, nanostructures engineered for light trapping via scattering mechanisms are also likely to provide some benefit from near-field enhancement.[9]

From an optical point of view, it is beneficial to have the plasmonic nanostructures in close proximity to the active material. Maximising the overlap of the concentrated near field with the absorber layer maximises both the coupling efficiency of scattered light and the absorption enhancement due to the enhanced fields. For example, minimising the thickness of spacer layers separating scattering rear-located metal nanoparticles from the semiconductor considerably increases the light trapping efficiency.[16,17] Similarly, over-coating embedded metal nanoparticles with thin dielectrics significantly reduces the efficiency of the absorption enhancement provided, unless the over-coating material is index-matched with the absorbing material.[15] However, the incorporation of nanostructures into a solar cell will strongly modify the carrier generation profile and it is necessary to take this into account when designing plasmonic light trapping structures.[18] In general, for bulk semiconductors, it is necessary to isolate the metal from the absorber to prevent increased recombination in the active layer.

In this report, we address the question: what are the electrical consequences, if any, of incorporating metal nanostructures inside semiconductor CQD films? We study simple photoconductor devices fabricated from PbS CQD films and incorporate periodic arrays of metal nanoparticles. Periodic arrays are employed to allow the calculation of the optical absorption enhancement in the films using full-field finite-dimension time-domain (FDTD) simulations for comparison with experiment. Three metals are chosen for the study: Au, Ag, and Al, all of which have been proposed as candidate materials for plasmonic light trapping structures. We demonstrate that direct contact with the metal nanoparticles leads to suppression or enhancement of the photocurrent depending on the work function of the metal. We attribute this to the alignment of the Fermi level of the metals with that of the p-type PbS QDs in the ultra-thin films. For the embedded Au nanoparticles, this provides a low resistance conduction channel for holes, increasing the effective mobility in the metal-semiconductor composite structure, and hence the responsivity. For Al and Ag nanoparticles, band bending at the interface results in depletion of the semiconducting film and a reduction in the responsivity. We discuss the implications of these effects, which can dominate over the optical effects of including the nanoparticles, for designing plasmonic light trapping for PbS CQD devices.

Colloidal PbS QDs were synthesised with a band gap, Eg of 1.3 eV, corresponding to an exciton peak at a wavelength of 950 nm. Figure 1(a) shows a schematic of the energy levels of a typical 3 nm PbS QD (Ref. 19) with respect to the work functions of the metals studied in this work. The relative thicknesses of the lines illustrate the estimated uncertainty in the work function of the metals due to differences in literature values and to degradation of the metal exposed to atmosphere, as discussed later. Figure 1(b) shows a schematic of the photoconductor geometry. Pairs of Au contact pads, of area $500 \times 500\,\mu$m and thickness 120 nm, were defined by standard photolithography techniques on quartz glass substrates, positioned 20 μm apart. Nanoparticle arrays were fabricated between the Au pads in the 20 μm gap using a lift-off procedure employing electron-beam lithography. PbS-CQD films were deposited using a "layer by layer" (LBL) process to build up the films to the desired thickness between the Au electrodes. In this way, we were able to measure current-voltage (I-V) and photocurrent spectra of the same device at two different thicknesses, roughly 60 nm (3 LBL) and 200 nm (10 LBL). Details of the chemical synthesis and the LBL deposition process are given in the supplementary information (SI).[25]

The parameters of the MNP arrays; i.e., period (L = 550 nm), particle radius (r = 200–250 nm), and height (h = 50 nm), were chosen to give high overall absorption enhancements based on predictions from FDTD simulations. Results and details of the optimisation procedure are given in the SI in Figure S5.

Scanning electron micrographs (SEMs) of the 3 different MNP arrays before PbS CQD film deposition are provided in Figure 2(a), along with the measured particle radii. The Ag MNP array shows signs of Ag degradation, which may affect the work function. From Ref. 20, the work function of evaporated Ag may vary from −4.5 to −5.0 eV due to exposure to atmosphere.[20] The striations visible in the SEMs are due to charging effects that are difficult to avoid when imaging insulating substrates.

Figure 2(b) shows transmission measurements of the three MNP arrays before PbS CQD film deposition (thick

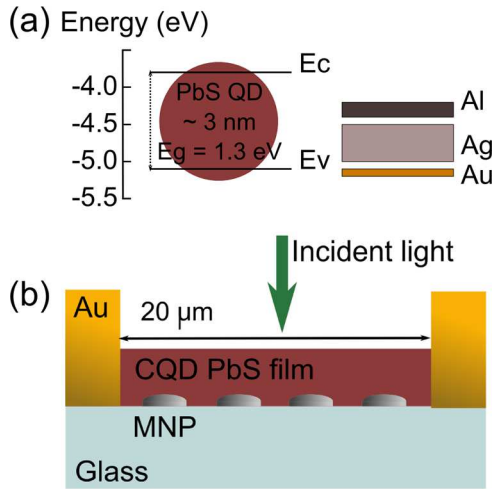

FIG. 1. (a) Schematic of the energy levels (conduction band (Ec), valence band (Ev), and band-gap (Eg)) of a typical PbS QD relative to the work functions of Au, Ag, and Al, as given by literature (see Ref. 19). (b) Schematic of the photoconductor geometry showing the embedded MNP array.

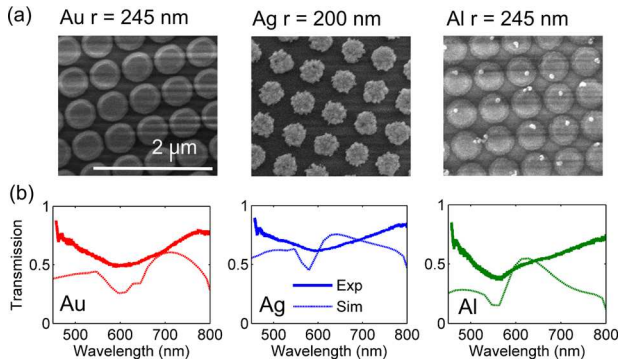

FIG. 2. (a) Scanning electron microscope images of the MNP arrays between the contacts, imaged before PbS CQD deposition. The measured radii are given for each array. (b) Transmission spectra of the metal nanoparticle arrays (thick lines, Exp) compared to calculated spectra from FDTD simulations (thin lines, Sim).

lines). Also plotted are transmission spectra from FDTD simulations of nanoparticle arrays on glass, with light incident from the air, and radii taken from the SEMs in Fig. 2(a). Further details of the simulation setup are reported in the SI along with full results in Figs. S3 and S4. The simulated spectra reproduce the dip in transmission observed in the experimental spectra as well as the trends of relative spectral position and strength for the 3 different metals. From Figs. s4(a), S4(d), and S4(g), it is clear that this dip corresponds to a second order short wavelength resonance. The main scattering plasmonic resonance occurs beyond a wavelength of 800 nm where lamp cuts off.

Current-voltage (I-V) characteristics and responsivity spectra at an applied voltage of 20 V were taken to characterise the devices after fabrication. Details of the optical and electrical measurements as well as the responsivity spectra are given in full in the SI and in Fig. S1.

Figures 3(a)–3(c) shows the responsivity enhancement, defined as the responsivity of a device with an embedded nanoparticle array relative to a similar device with no embedded nanoparticle array, for photoconductors of thickness ~60 nm (3 LBL), for the three different MNP arrays shown in Figure 2 (thick lines). Also plotted are calculated absorption enhancements from FDTD simulations of MNP arrays embedded in the PbS CQD films (dashed lines). The full simulation details and results are given in the SI and Figs. S4(b), S4(e), and S4(h).

The measured enhancement spectra show that embedded Au particles (Fig. 3(a)) result in large broadband enhancements, of up to factor 7. For embedded Ag nanoparticles (Fig. 3(b)), modest enhancements are observed at wavelengths around 800 nm and beyond 1100 nm, while suppression occurs at other wavelengths. For the Al particles (Figs. 3(e) and 3(f)), the responsivity is significantly suppressed to below half of the value of the reference case at all wavelengths.

From the optical simulations, Ag particles give the highest absorption enhancements, up to a factor of 6. The calculated absorption enhancements for the 3 different metals (thin lines Figs. 3(a)–3(c)) do not reproduce the measured responsivity enhancements. The optical simulations predict less enhancement for Au at all wavelengths and more enhancement for Al and Ag. Additionally, enhancements

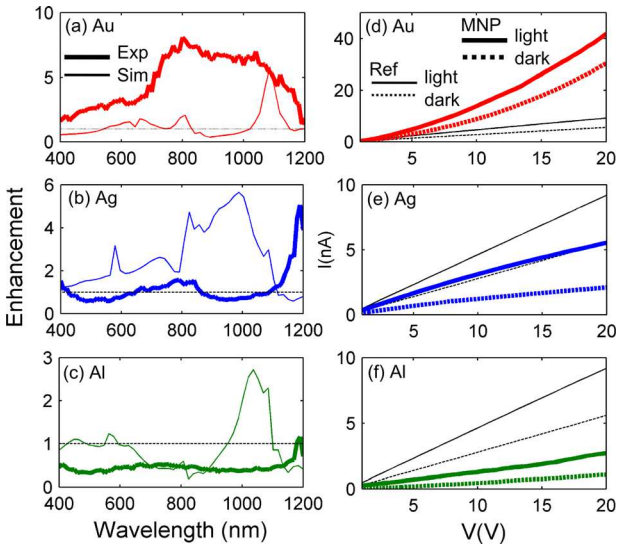

FIG. 3. (a)-(c) Responsivity enhancements for photoconductors with (a) Au, (b) Ag, and (c) Al embedded MNP arrays (thick lines), calculated as responsivity relative to a similar device with no embedded nanoparticle array. For comparison, simulated absorption enhancements (thin lines) are given for similar structures in each case. A dashed line at enhancement = 1 is given as a guide to the eye. (d)-(f) Current-voltage curves for photoconductors with Au (d), Ag (e), and Al (f) embedded MNP arrays (thick lines). Data are shown for devices under illumination at a wavelength of 635 nm (solid lines) and in the dark (dashed lines). For reference, data are also given for a photoconductor of similar thickness without embedded MNPs (thin lines).

(suppression) for the Au (Al) particles occur at all wavelengths. These results suggest that a non-optical mechanism is dominating the effect of MNP arrays on the responsively.

To investigate electrical conduction in the MNP sensitised photoconductors, we monitored the current voltage (I-V) characteristics of the devices. Figures 3(d)–3(f) shows the I-V curves for the photoconductors in the dark (dashed lines) and under illumination at a wavelength of 635 nm (solid lines). The references (black lines) show typical linear I-V characteristics of a PbS CQD photoconductor. Embedded Au MNPs increase both the light and dark current by a factor of 4.5 (light) and 5.5 (dark) at 20 V (Fig. 3(d)). Additionally, the dependence of current on voltage is super-linear. Conversely, Ag MNPs *decrease* both the light and dark current by a factor of 0.6 (light) and 0.4 (dark) and demonstrate sub-linear I-V curves (Fig. 3(e)). Al MNPs also strongly decrease light and dark current, by 0.3 (light) and 0.2 (dark) (Fig. 3(f)).

We attribute the observed I-V characteristics demonstrated by photoconductors with embedded MNP arrays to the alignment of the Fermi level of the metals with that of the p-type PbS QDs in the ultra-thin films.

For Au MNPs, the work function of the nanoparticles is aligned with the valence band (Ev) of the PbS QDs, as shown schematically in Figure1(a). This allows charge transfer to occur easily between the semiconductor and the metal. In other words, the metal nanoparticles allow the formation of a low resistance pathway in their vicinity, increasing the mobility of the carriers as they flow through the device under the applied bias, as shown schematically in Figure 4.

For Ag and Al MNPs, the work function of the metal is at a lower energy than the Fermi level of the PbS QDs and both metals form Schottky junctions with p-type PbS CQD films.[21] The built-in voltage (V_{bi}) and the width of the resulting depletion region (W) can be estimated in a simple manner using the equations for an ideal Schottky junction.[22] The results are given in Table I. Here, the work function of the p-type PbS CQD films, $|\Psi_{PbS}| = 4.9$ eV, the DC dielectric function, $\epsilon_{PbS} = 18$, and the carrier density, $N_{PbS} = 8 \times 10^{16}\,cm^{-3}$, are taken from literature values for ~3 nm PbS QDs, synthesised in a similar manner.[19,21]

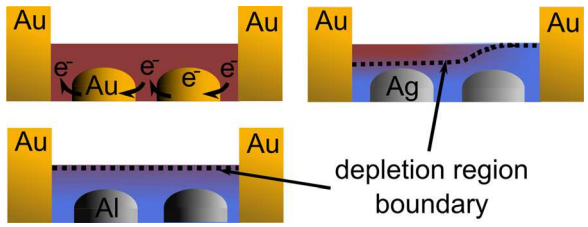

FIG. 4. Schematic of effects of MNP inclusion in ultra-thin PbS CQD for 3 the different metals. For Au embedded MNPs, the particles provide a low resistance pathway for current conduction. For Ag and Al MNPs, a depletion region is set up, delineated by a dashed line. With embedded Ag particles, the film is partially depleted and application of an external bias leads to an increase in the depletion region width at one electrode.

From this calculation, we expect the PbS CQD film with embedded Al MNPs to be fully depleted for t = 60 nm. The degree of depletion due to the Ag MNPs depends on the work function, and hence the degradation of the MNPs. To confirm this hypothesis, Kelvin probe measurements were performed on large area (1 cm × 1 cm) PbS CQD films on glass with and without embedded Au, Ag, and Al nanoparticle films. Since it is not feasible to use electron beam lithography to fabricate such large area arrays, random nanoparticles were fabricated by evaporation of thin films of metal (20 nm Au, 15 nm Ag, and 20 nm Al) on glass slides followed by an annealing step (1 h at 350 °C for Au and 250 °C for Ag and Al) in an inert N_2 atmosphere. This fabrication method results in MNPs 30–50 nm in height and with diameters of 100–200 nm.[5,23] The differences in the fabrication techniques for random and periodic particles studied here may affect the work function of the resulting nanoparticles, within the range shown in Fig. 1. The electrical effect of embedded nanoparticles will be similar, independent of the details of the array configuration, as long as the area densities of the nanoparticles are similar. For the arrays studied here, the area densities are within the range 30%–50% for both the random and periodic nanoparticle arrays. The PbS CQD films were deposited as before by the LBL method. Thicker films with 10 LBL were also fabricated, resulting in film thicknesses of roughly 200 nm. The work functions of the films were measured in the dark using a Kelvin Probe set-up with the tip calibrated with respect to Au with work function $|\Psi| = 5.1$ eV. The results are given in Table II.

TABLE I. Calculated built in voltage (V_{bi}) and depletion region (W) for ideal PbS CQD metal Schottky junctions. The following parameters are taken from Refs. 19 and 21: work function of the p-type PbS CQD, $|\Psi_{PbS}| = 4.9$ eV, the DC dielectric function, $\varepsilon_{PbS} = 18$, and the carrier density, $N_{PbS} = 8 \times 10^{16}\,cm^{-3}$.

	$\lvert\Psi_m\rvert$ (eV)	$V_{bi} = \lvert\Psi_m\rvert - \lvert\Psi_{PbS}\rvert$ (eV)	$W = \sqrt{2\varepsilon_{PbS}\varepsilon_0 V_{bi}/qN_{PbS}}$ (nm)
Ag	4.3–5.0	0.6–0.0	122–0
Al	4.1–4.2	0.8–0.7	141–132

TABLE II. Measured work functions for PbS CQD films with and without embedded films of random MNPs.

Sample	3 LBL |Ψ| (eV)	10 LBL |Ψ| (eV)
PbS	4.9	4.9
PbS + Au MNPs	4.9	4.9
PbS + Ag MNPs	4.6	4.9
PbS + Al MNPs	4.7	4.9

The Ag and Al MNPs reduce the work function of the 3 LBL PbS CQD film, due to depletion of the PbS CQD layer. For thicker films, the work function of the PbS CQD recovers. As expected, the work function of the semiconductor is unaffected by the Au MNPs.

We attribute the non-linear IV curves of photodetectors with embedded Ag and Al MNPs in Figs. 3(c)–3(f) to the formation of non-Ohmic contacts due to the change in the Fermi level of the depleted PbS CQD films. Decreasing the work function of the PbS CQD leads to the creation of back-to-back Schottky junctions at the PbS CQD/Au contacts. For Al MNPs, the PbS CQD film is strongly depleted and the IV characteristics, shown in Fig. 3(f), are markedly similar to those of a plain PbS CQD photodetector with Ag contacts forming back-to-back Schottky junctions (shown in Fig. S6 for comparison). For devices with Ag MNPs, the IV curve show sub-linear behaviour in Fig. 3(e). Here, the PbS CQD is only partially depleted and a conduction channel is formed, as illustrated in Figure 4. Increasing the bias reduces the length of the channel and results in sub-linear dependence of current on voltage.

To study the effect of thickness on the charge transport in MNP sensitised photoconductors, additional LBL depositions were performed resulting in 10 LBL films, which were 200 nm thick. The IV curves of these devices are given in Figs. S2(b), S2(d), and S2(f)). For the 200 nm thick Ag MNP sensitised devices, in Fig. S2(d), the reduction in the dark current is less severe and the IV curves are more linear compared to the thinner 3 LBL case. As the thickness of the CQD PbS films increases, the fraction of the film that is depletion is reduced and electrical effect of the nanoparticles decreases. This is consistent with previously published work in which we demonstrate optical enhancement of 200–450 nm thick CQD PbS photoconductors due to scattering from random Ag particle arrays.[5] For the 200 nm Al case, Fig. S2(f), the film is partially depleted (consistent with the calculation in Table I) and a conduction channel is formed, resulting in sub-linear I-V curves similar to the 3 LBL Ag case.

In the above discussion, we have assumed that the metal MNP-PbS CQD Schottky junctions have bulk electrical characteristics. However, it has been shown that the Schottky junction barrier height becomes a function of the finite volume of the metal and is reduced if the radius of the metal nanoparticle is significantly smaller than the characteristic length for the junction, l_c.[24] Following the work of Smit and colleagues in Ref. 24, we calculate $l_c = \sqrt{2\epsilon_{PbS}V_{bi}/qN_{PbS}} < 60$ nm for the Schottky junctions discussed in this work. The metal structures studied here have $100 < d < 250$ nm and can be assumed to form bulk-like Schottky junctions. However, for MNPs with radii much smaller than l_c, which may be employed for near-field enhancement studies,[14,15] the effect of the finite metal volume should be taken into account. For structures larger than the characteristic length scale of the junction, the electrical effects of embedding metal nanoparticles inside ultra-thin PbS CQD films are independent of the particle shape, size, and array structure (for similar area densities).

In summary, we have demonstrated that the electrical effects of incorporating metal nanoparticles in ultra-thin PbS CQD films can dominate the optical effects and can enhance or supress the current depending on the work function of the metal. These results have implications for the design of plasmonic optoelectronics. Incorporating metal nanostructures into more complex devices, such as solar cells or photodetectors, could change the nature of existing p-n junctions and/or the type of electrical contact formed, depending on the position of the nanoparticles within the device and the work function of the metal.

This research has been supported by Fundacio′ Privada Cellex Barcelona and the European Commission's Seventh Framework Programme for Research under contract PIRG06-GA-2009-256355 and the Ministerio de Ciencia e Innovacion under Contract No. TEC2011-24744. The authors would like to thank Dr. Silke Diedenhofen for useful discussions, Pablo Manuel de Roque for assistance with the transmission measurements and Rafael Betancur for assistance with the Kelvin Probe measurements.

[1]D. V. Talapin, J.-S. Lee, M. V. Kovalenko, and E. V. Shevchenko, Chem. Rev. **110**, 389–458 (2010).
[2]G. Konstantatos and E. H. Sargent, Nat. Nanotechnol. **5**, 391–400 (2010).
[3]G. Konstantatos, I. Howard, A. Fischer, S. Hoogland, J. Clifford, E. Klem, L. Levina, and E. H. Sargent, Nature (London) **442**, 180–183 (2006).
[4]A. D. R. Barkhouse, R. Debnath, I. J. Kramer, D. Zhitomirsky, A. G. Pattantyus-Abraham, L. Levina, L. Etgar, M. Grätzel, and E. H. Sargent, Adv. Mater. **23**, 3134–3138 (2011).
[5]F. P. García de Arquer, F. J. Beck, M. Bernechea, and G. Konstantatos, Appl. Phys. Lett. **100**, 043101 (2012).
[6]K. R. Catchpole, S. Mokkapati, F. Beck, E.-C. Wang, A. McKinley, A. Basch, and J. Lee, MRS Bull. **36**, 461–467 (2011).
[7]Z. Ouyang, S. Pillai, F. Beck, O. Kunz, S. Varlamov, K. R. Catchpole, P. Campbell, and M. A. Green, Appl. Phys. Lett. **96**, 261109 (2010).
[8]V. E. Ferry, J. N. Munday, and H. A. Atwater, Adv. Mater. **22**, 4794–4808 (2010).
[9]R. A. Pala, J. White, E. Barnard, J. Liu, and M. L. Brongersma, Adv. Mater. **21**, 3504–3509 (2009).
[10]D. Derkacs, S. H. Lim, P. Matheu, W. Mar, and E. T. Yu, Appl. Phys. Lett. **89**, 093103 (2006).
[11]I.-K. Ding, J. Zhu, W. Cai, S.-J. Moon, N. Cai, P. Wang, S. M. Zakeeruddin, M. Grätzel, M. L. Brongersma, Y. Cui, and M. D. McGehee, Adv. Eng. Mater. **1**, 52–57 (2011).
[12]S. Pillai, K. R. Catchpole, T. Trupke, and M. A. Green, J. Appl. Phys. **101**, 093105 (2007).
[13]B. P. Rand, P. Peumans, and S. R. Forrest, J. Appl. Phys. **96**, 7519 (2004).
[14]J.-Y. Lee and P. Peumans, Opt. Express **18**, 10078–10087 (2010).
[15]F. P. García de Arquer, F. J. Beck, and G. Konstantatos, Opt. Express **19**, 21038–21049 (2011).
[16]S. Pillai, F. J. Beck, K. R. Catchpole, Z. Ouyang, and M. A. Green, J. Appl. Phys. **109**, 073105 (2011).
[17]F. J. Beck, S. Mokkapati, and K. R. Catchpole, Opt. Express **19**, 25230–25241 (2011).
[18]X. Li, N. P. Hylton, V. Giannini, K.-hua Lee, N. J. Ekins, and S.A. Maier, Opt. Express **19**, 888–896 (2011).
[19]J. Tang, L. Brzozowski, A. D. R. Barkhouse, X. Wang, R. Debnath, R. Wolowiec, E. Palmiano, L. Levina, A. G. Pattantyus-Abraham, D. Jamakosmanovic, and E. H. Sargent, ACS Nano **4**, 869–878 (2010).

[20]J. B. Kim, C. S. Kim, Y. S. Kim, and Y.-L. Loo, Appl. Phys. Lett. **95**, 183301 (2009).
[21]A. G. Pattantyus-Abraham, Ḱ. I. J. Kramer, A. D. R. Barkhouse, X. Wang, G. Konstantatos, R. Debnath, L. Levina, I. Raabe, M. K. Nazeeruddin, and E. H. Sargent, ACS Nano **4**, 3374–3380 (2010).
[22]S. M. Sze, *Semiconductor Physics and Devices*, 2nd ed. (Wiley, 2002), p. 225.
[23]H. R. Stuart and D. G. Hall, Appl. Phys. Lett. **69**, 2327–2329 (1996).
[24]G. D. J. Smit, S. Rogge, and T. M. Klapwijk, Appl. Phys. Lett. **81**, 3852 (2002).
[25]See supplementary material at http://dx.doi.org/10.1063/1.4738993 for further details of the colloidal quantum dot synthesis, the layer by layer deposition technique and the simulation setup, as well as additional supporting results.